Front. Phys., 2011, 6(4): 398–409
DOI 10.1007/s11467-011-0214-z

MINI-REVIEW ARTICLE

Vortex lattices in type-II superconductors studied by small-angle neutron scattering

Morten Ring Eskildsen

Department of Physics, University of Notre Dame, Notre Dame, IN 46556, USA

E-mail: eskildsen@nd.edu

Received September 13, 2011; accepted September 20, 2011

Here we review recent small-angle scattering studies of the vortex lattice in a range of type-II superconductors carried out by our group. Emphasis is placed on providing examples of the kind of information which can be obtained by such measurements, focusing in particular on studies of the vortex lattice structure and form factor in $LuNi_2B_2C$, $TmNi_2B_2C$, $CeCoIn_5$ and $Ba(Fe_{0.93}Co_{0.07})_2As_2$.

Keywords superconductivity, vortex lattice, small-angle neutron scattering, borocarbides, pnictides, $CeCoIn_5$

PACS numbers 74.25.Uv, 74.25.Wx, 61.05.fg, 74.70.Dd, 74.70.Tx, 74.70.Xa

Contents

1 Introduction

When a type-II superconductor is subjected to a magnetic field it is threaded by vortices each carrying one quantum of magnetic flux, ϕ_0. At the core of the vortices the superconducting order parameter is suppressed over a length scale given by the superconducting coherence length (ξ). Encircling the vortex core supercurrents extend to a distance given by the penetration depth (λ), seeking to screen the magnetic field from the rest of the material.

In the absence of pinning the vortices will arrange themselves in a periodic array, the vortex lattice (VL), due to their mutual repulsion. Studies of the VL can provide a wealth of information about not only the VL itself, but also about the detailed nature of the superconducting state in the host material.

Here we review recent small-angle neutron scattering (SANS) studies of the VL in a range of type-II superconductors carried out by the Notre Dame group and its collaborators. We present measurements on members of the nickelborocarbides, the heavy fermion superconductor $CeCoIn_5$ and the recently discovered iron-pnictide material $Ba(Fe_{0.93}Co_{0.07})_2As_2$. The emphasis will be on a description of the various VL properties which can be investigated by SANS, irrespective of whether the specific superconductor is considered conventional or exotic.

2 Small-angle neutron scattering

There exists a wide range of experimental techniques which allow the imaging of vortices in type-II superconductors. With the exception of scanning tunneling microscopy (STS), which uses local measurements of the presence or absence of a superconducting gap in the electronic density of states, these rely on the modulation of the magnetic field arising from the presence of the vortices. Since the fractional field modulation decreases rapidly with increasing field and the distance from the sample surface, direct space surface-sensitive techniques such as Bitter decoration, scanning-SQUID microscopy and magnetic force microscopy (MFM) are limited to small fields, typically no more than a few milliTesla.

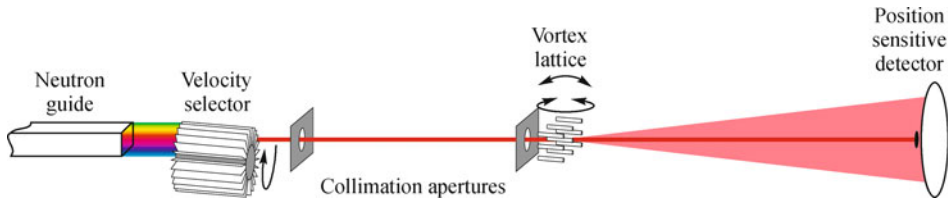

Fig. 1 Schematic diagram of a typical small-angle neutron scattering setup for vortex lattice studies.

Among bulk techniques, muon spin rotation (μSR) is directly sensitive to the distribution of field values within the mixed state, and is only limited at high fields by the difficulty of getting the muon and its decay positron into and out of the sample. However, μSR is not directly sensitive to the VL shape or disorder, requiring assumptions about these to model and interpret the data [1]. Finally, the results may also be affected by local magnetic order [2].

Small-angle neutron scattering utilizes that the neutrons have a spin and correspondingly a magnetic moment. As a result, they experience a varying magnetic potential energy due to the VL which leads to diffraction. As SANS is sensitive to the variation of the magnetic field rather than the average value, it is possible to perform measurement at high fields with relative field modulations $< 10^{-3}$. Recent examples of high field VL imaging by SANS include $CeCoIn_5$ up to 10.9 T [3] and YBCO up to 16.7 T [4, 5]. Furthermore, SANS has the advantage of being a bulk probe, sampling the VL in the entire sample, and is as such not subject to the same severe requirements concerning the sample surface quality as for example STS. On the other hand SANS does require a relatively well-ordered VL, which in the case of the iron-based superconductors has proved to be a severe limitation.

A schematic diagram of a typical SANS setup is shown in Fig. 1. The neutrons first pass through a velocity selector which determines the average wavelength as well as the bandwidth (typically $\sim 10\%$ FWHM). The beam is then collimated before it interacts with the sample. The most common configuration is with the magnetic field (and hence the vortices) along the incoming neutron beam. As "cold" neutrons have a wavelength in the range $\lambda_n = 0.2 - 2$ nm and the vortex spacing varies between ~ 10 and ~ 400 nm (corresponding to 15 T and 10 mT respectively), the scattering angles are typically of the order one degree or less. To obtain diffraction from the VL, one therefore needs only to rotate and/or tilt the magnet and sample by very small angles in order to satisfy the Bragg condition for the VL planes. Following the sample is a long evacuated flight path, which allows the diffracted neutron to be spatially separated from the unscattered beam. Finally the scattered neutrons are collected by a two-dimensional position sensitive detector while the unscattered beam is caught on a neutron-absorbing beamstop.

In the following we review examples that illustrate the kind of information one can obtain from SANS studies of the VL.

3 Vortex lattice structure

Figure 2 shows a VL diffraction pattern obtained in the nickelborocarbide superconductor $LuNi_2B_2C$. This is the sum of measurements at a number of different angles to construct an image of the VL in reciprocal space (more about the angular dependence of the scattered intensity will follow in Section 4). Due to the two-dimensional nature of the VL, the real-space unit cell is obtained by simply rotating the first order diffraction spots by 90° about the main beam and adding one vortex at the center of the image ($q = 0$). For the diffraction pattern in Fig. 2 one thus concludes that this corresponds to a square VL with the nearest neighbors in the crystalline ⟨110⟩ directions.

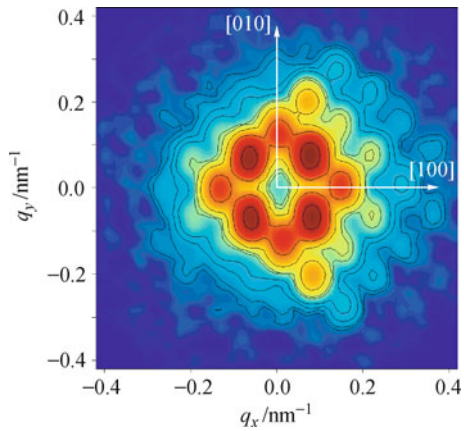

Fig. 2 Example of small-angle neutron scattering from the VL in $LuNi_2B_2C$ at 2 K and with a magnetic field of 0.5 T applied parallel to the crystalline c-axis. A large number of measurement angles were added to show many higher order reflections for the square VL in the center-right part of the detector. The data are smoothed and shown on a logarithmic intensity (color) scale. Measurements at 6 T, where no scattering from the VL could be observed, were used for background subtraction. The arrows indicate the orientation of the crystalline axes in the tetragonal basal plane. Reproduced from Ref. [6], Copyright © 2009 American Physical Society.

Since the VL in isotropic superconductors is expected to be hexagonal [7, 8], any other symmetry will reflect an anisotropy of the plane perpendicular to the applied field

coupled with non-local electrodynamics. Possible origins of such anisotropies include the Fermi surface and the superconducting gap [9–13]. Moreover, since the ability of these anisotropies to affect the VL structure decreases with increasing vortex separation, one commonly finds a hexagonal VL at low fields which undergoes a transition to a square symmetry as the field is increased. Materials where such a field-driven hexagonal to square VL transition have been observed includes members of the nickelborocarbide superconductors [14–22], V_3Si [23, 24], LSCO [25], $CeCoIn_5$[26, 27], YBCO [4, 28], and NCCO [29]. Notable exceptions to this are BSCCO [30, 31], and more recently $HgBa_2CuO_{4+\delta}$ [32]. However, in these two compounds the scattered intensity decreases very rapidly with increasing field, greatly limiting the range of vortex densities over which the VL can be imaged.

In materials where a well-ordered vortex lattice is observed, the magnitude of the scattering vector of the first-order Bragg reflection is determined not only by the magnitude of the applied field but also by the symmetry of the VL. In the case of a rhombic lattice, i.e., oblique with equal side lengths but an arbitrary opening angle $60° < \beta < 90°$, the scattering vector is given by

$$q_{10} = 2\pi\sqrt{\frac{B}{\phi_0 \sin\beta}} \tag{1}$$

whereas a distorted hexagonal lattice ($\beta < 60°$) will have

$$q_{10} = 2\pi\sqrt{\frac{2B}{\phi_0 \tan\beta/2}} \tag{2}$$

Here B is the magnetic field and $\phi_0 = h/(2e) = 2070$ Tnm^2 is the flux quantum. Especially, high symmetry cases include $\beta = 60°$ (or 120°) and $\beta = 90°$ corresponding to a hexagonal and square VL respectively, with $q_{\rm hex} = (2/\sqrt{3})^{1/2}\, q_{\rm sq}$.

3.1 VL transitions in $CeCoIn_5$

In Fig. 3 we show a sequence of VL diffraction patterns obtained in the $CeCoIn_5$ with increasing field. This material is a heavy-fermion superconductor with a critical temperature $T_c = 2.3$ K [34]. Panels (a)–(c) show the usual evolution from a distorted hexagonal ($\beta \approx 56°$) to a rhombic ($\beta = 68° - 90°$) and finally a square VL. In the case of $CeCoIn_5$ the square VL is believed to be stabilized by the four-fold $d_{x^2-y^2}$ symmetry of the superconducting order parameter [35, 36]. Here one notes that when the symmetry of the VL differs from that of the host material, which is tetragonal, several degenerate VL orientations are possible. In the case of the hexagonal VL in panel (a) a total of $2 \times 6 = 12$ Bragg reflections are observed, corresponding to scattering from a roughly equal mixture of two different domain orientations with the nearest neighbor directions aligned along the [110] and [1$\bar{1}$0] crystalline directions respectively. Similarly, the diffraction pattern in panel (b) consists of $2 \times 4 = 8$ reflections from two rhombic domains.

What is highly unusual about the VL in $CeCoIn_5$ is that the square VL phase is found to be re-entrant upon further increases of the magnetic field as seen in Figs. 3(d) and (e). This shows the VL returning to first a rhombic (d) and finally a near hexagonal (e) symmetry. The phase diagram in Fig. 4 summarizes the VL symmetry in this compound. The re-entrance of the square VL phase is indicative of a decreasing four-fold anisotropy of the plane in which the screening currents are circulating, and that this decrease occurs faster than the effect of the increasing vortex density. The origin of this is believed to be the strong Pauli paramagnetic effects observed in $CeCoIn_5$ which causes the vortex cores to expand and become more isotropic at fields approaching H_{c2}. This effect also manifests itself in measurements of the VL form factor as we will describe in Section 4. Finally, we note that a qualitatively similar evolution of the VL was observed in $TmNi_2B_2C$ which also exhibits Pauli paramagnetic effects [37, 38].

3.2 Disordered vortex configurations in $Ba(Fe_{0.93}Co_{0.07})_2As_2$

As mentioned in the introduction, in order to use SANS for vortex imaging a well-ordered VL is required. In a perfect crystal the Bragg spots become delta functions (broadened only by the experimental resolution) which contain all of the diffracted intensity. As disorder increases the scattered intensity will spread out in reciprocal space, eventually making it difficult or impossible

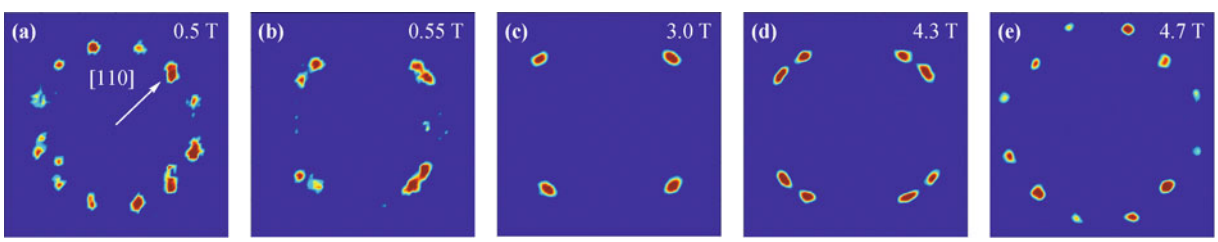

Fig. 3 Diffraction patterns in $CeCoIn_5$ at 50 mK for a range of fields from 0.5 to 4.7 T and showing hexagonal **(a, e)**, rhombic **(b, d)** and square **(c)** VL symmetries. The orientation of the crystalline lattice is shown in panel (a). Reproduced from Refs. [27, 33], Copyright © 2006 American Physical Society and Copyright © 2008 American Association for the Advancement of Science respectively.

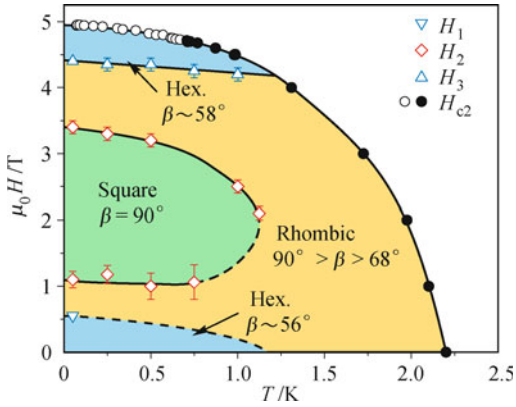

Fig. 4 Structural phase diagram for the VL in $CeCoIn_5$ with the field applied parallel to the four-fold c-axis. Below 0.7 K the transition from the superconducting to the normal state becomes first order (shown by open circles) due to Pauli paramagnetic limiting. Reproduced from Ref. [33], Copyright © 2008 American Association for the Advancement of Science.

to detect. The effect of disorder and the classification of the VL as a so-called Bragg glass in well ordered systems have been reported elsewhere [39–41]. Here we will focus on our recent studies of the highly disordered vortex configuration in a member of the iron-pnictide superconductors.

Figure 5 shows a diffraction pattern obtained in $Ba(Fe_{0.93}Co_{0.07})_2As_2$ with the applied field almost parallel to the crystalline c-axis. This shows a vortex "powder diffraction" ring of scattering instead of well defined Bragg peaks, indicating that orientational order is lost. Furthermore, the scattered intensity is spread over very large rocking angles (not shown) implying that rather than being straight the vortices "wander" significantly on their way through the sample. Similar results were found by direct space vortex imaging techniques. Bitter decoration and MFM measurements at low fields which showed small ordered domains extending a few vortex

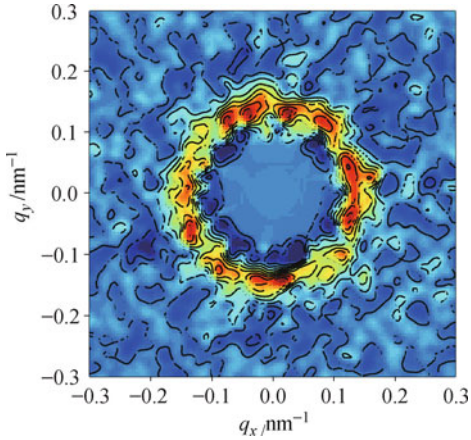

Fig. 5 SANS diffraction pattern showing a ring of scattering from the vortices in $Ba(Fe_{0.93}Co_{0.07})_2As_2$ at 2 K and 1 T. The measurement was performed at a single (centered) orientation of the magnetic field with respect to the neutron beam direction, and background measurements were subtracted. The data is smoothed and the central part of the detector is masked off. Reproduced from Ref. [42], Copyright © 2010 Institute of Physics.

spacings and interspersed with regions of disordered vortices [43–45], and STS imaging in $BaFe_{1.8}Co_{0.2}As_2$ at very high fields also found a disordered vortex configuration [46]. This shows that a large degree of what is most likely intrinsic vortex pinning is present in Co-doped $BaFe_2As_2$.

Despite the disorder the well-defined ring of scattering shows that the intervortex distance, a, remains relatively uniform throughout the sample. Furthermore, as the field is increased this spacing decreases, causing the ring of scattering to expand since $q_{10} \propto 2\pi/a \propto (B/\phi_0)^{1/2}$. This is illustrated in Fig. 6(a), which shows the radial intensity distribution with increasing field. Here each intensity distribution has been fitted to a Gaussian

$$I = I_0 \exp\left[-\frac{(q-q_p)^2}{2\sigma_q^2}\right] \quad (3)$$

which makes it possible to obtain a quantitative measure of the magnitude of the scattering vector (q_p), the radial width of the scattering (σ_q) and the total scattered intensity (I_0). Here we will focus only on the first two quantities since an accurate measurement of I_0

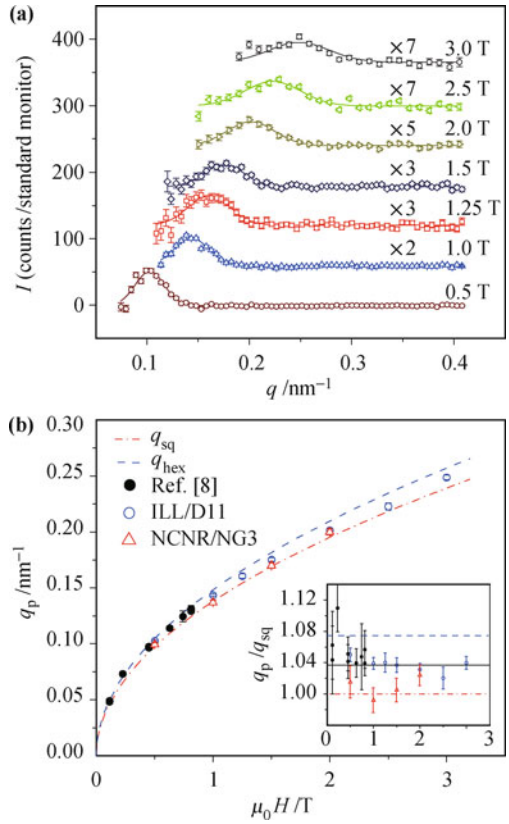

Fig. 6 Scattering vector magnitude in $Ba(Fe_{0.93}Co_{0.07})_2As_2$. **(a)** Radial intensity distribution at 2 K as a function and applied magnetic fields between 0.5 to 3 T, with Gaussian fits to the data at each field. **(b)** Field dependence of the measured scattering vector, q_p, given by the maximum of the fits in panel (a). The scattering vectors expected for respectively a square (*dashed lines*) and a hexagonal (*dot-dashed lines*) VL are shown for comparison. The insert shows measured scattering vector normalized to q_{sq}. The solid line is the average $q_p/q_{sq} = 1.037 \pm 0.003$. Reproduced from Ref. [42], Copyright © 2010 Institute of Physics.

requires an integration of the scattered intensity as it is rocked through the Ewald sphere, something which was not possible in $Ba(Fe_{0.93}Co_{0.07})_2As_2$ due to the strong disorder.

A comparison of the measured scattering vector to those expected for respectively a square (q_{sq}) and a hexagonal (q_{hex}) symmetry is shown in Fig. 6(b). The measured scattering vectors fall between q_{hex} and q_{sq}, with no apparent field dependence of the normalized scattering vector shown in the insert. Given the tetragonal crystal structure of $Ba(Fe_{0.93}Co_{0.07})_2As_2$ one would expect a transition to a square VL with increasing field. Possible explanations for the absence of any clear features in q_p/q_{sq} includes a short non-locality range which will broadens a symmetry transition and shift it to higher fields [20], or simply that the transition occur above the highest measured field similar to what have been observed in YBCO where a square VL is only obtained in fields exceeding 10 T [4, 28]. In the case of $Ba(Fe_{0.93}Co_{0.07})_2As_2$ the magnitude of the scattering vector can also reflect a completely disordered vortex arrangement without any short range order and with an average vortex separation slightly exceeding that of a close packed hexagonal symmetry, which would also lead to $q_p < q_{hex}$. However, a square VL coordination can be ruled out. Despite these limitations it is interesting to use the average $q_p/q_{sq} = 1.037$ together with Eqs. (1) and (2) to evaluate corresponding opening angles of $\beta \approx 68°$ and $\approx 56°$ respectively. The latter value compared favorably with the measurements of the VL in KFe_2As_2 which is the only member of the ferro-pnictide superconductors where a well-ordered VL have been observed [47].

We now turn to the width of the radial intensity distribution (σ_q). As shown in Fig. 7 this is found to increase monotonically with the magnetic field, exceeding the experimental resolution (σ_r) at all fields, with the two converging only in the limit of zero applied field. The difference between σ_q and σ_r can be used to estimate the radial VL correlation length,

$$\zeta = 1/\sqrt{\sigma_q^2 - \sigma_r^2} \tag{4}$$

Over the range of measured fields the correlation length is found to follow a power law behavior $\zeta = 79\ \text{nm}\ (H/[\text{T}])^{-0.6}$. With an exponent close to $-1/2$, the ratio of the correlation length to the intervortex spacing is essentially independent of field, yielding $\zeta/a = 1.8 \pm 0.2$. Similar results were found in Bitter decoration experiments performed in applied fields of a few mT [43, 44], indicating strong single-vortex pinning over a wide range of magnetic fields in $Ba(Fe_{0.93}Co_{0.07})_2As_2$. This is consistent with the extrapolated radial width reaching the resolution limit at $H = 0$. The same conclusion was reached by Inosov *et al.* [45].

Apart from Co-doped $BaFe_2As_2$, VL studies have been reported for two other members of the iron-based superconductors: LiFeAs and $(Ba,K)Fe_2As_2$. In the case of the 111-compound LiFeAs, a disordered VL was observed as indicated by a "powder ring" of scattering from the vortices [48]. However, in contrast to the results for $Ba(Fe_{0.93}Co_{0.07})_2As_2$ presented above, a well-defined rocking curve could be measured, indicating weaker pinning in LiFeAs and allowing an analysis of the total scattered intensity (see Section 4). Given the sensitivity to the air and the difficult handling required for LiFeAs, it is possible that further advancements in sample preparation and mounting will lead to improved SANS results in future experiments. In the case of K-doped $BaFe_2As_2$, a well-ordered VL was observed by SANS in the pure potassium compound KFe_2As_2 [47, 49]. Similarly, vortex imaging by STS in optimally doped $Ba_{0.6}K_{0.4}Fe_2As_2$ revealed an ordered VL at relatively high fields (4 and 9 T) albeit within a relatively limited field of view [50]. An extensive review of VL SANS studies in the iron-based superconductors can be found in Ref. [51].

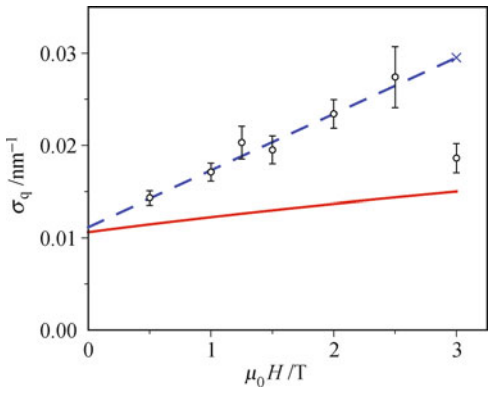

Fig. 7 Width of Gaussian fits to the radial intensity distributions shown in Fig. 6(a). The dashed line is a linear fit to the data (excluding the anomalously low width at 3 T). The calculated resolution is shown by the full line. Reproduced from Ref. [42], Copyright © 2010 Institute of Physics.

4 Vortex lattice form factor

Measuring the intensity of the VL reflections as the sample is rotated around the vertical or horizontal axis to satisfy the Bragg condition provides rocking curves such as the ones shown in Fig. 8(a). These correspond to two of the Bragg spots in the diffraction pattern in Fig. 2. Here the different reflections are located at distances from the center of the detector which are proportional to the magnitude of their scattering vector, $q_{hk} = (h^2 + k^2)^{1/2} q_{sq}$. In addition to the strongest (10) reflection, Fig. 2(a) also shows the (32) rocking curve which was the highest order reflection visible in $LuNi_2B_2C$ in a field of 0.5 T. The longer scattering vector for the (32) reflection, $q_{32} = \sqrt{13}\, q_0$, is evident by the larger rotation angle necessary to satisfy the Bragg condition.

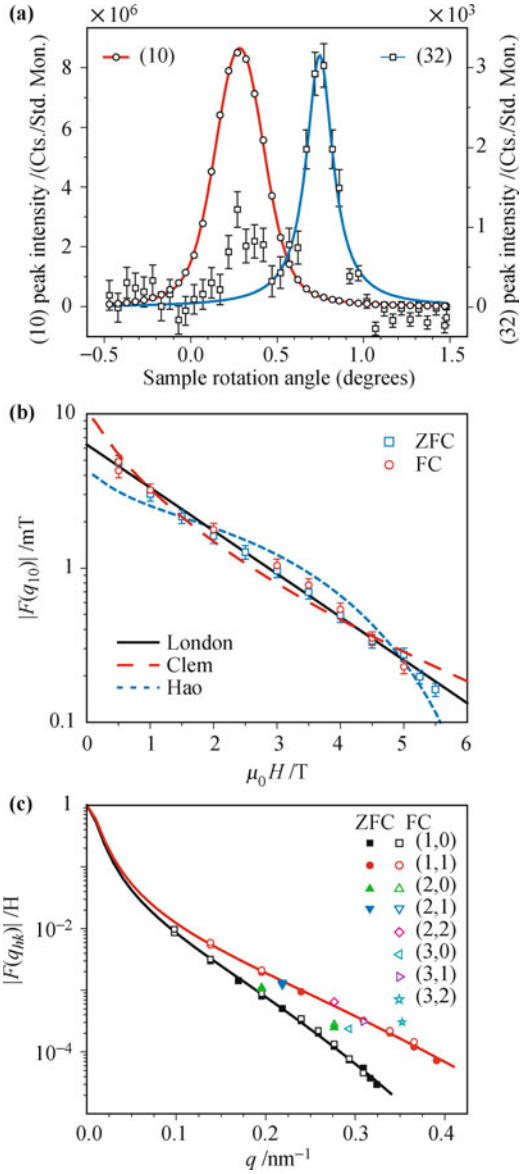

Fig. 8 Measurements of the VL form factor in $LuNi_2B_2C$. **(a)** Rocking curves at 0.5 T and 2 K for the (10) and (32) VL reflections from Fig. 2. Note the different intensity scales for the two reflections. The intensity at each angular setting are obtained by summing up the detector counts at the position of the specific Bragg reflection. The curves are Voigt fits to the data. **(b)** Field dependence of the VL (10) form factor for both the field cooled (FC) and zero field cooled (ZFC) case. **(c)** VL form factor divided by the applied field versus scattering vector q for all measured reflections. Curves through $|F(q_{10})|$ and $|F(q_{11})|$ are fits to the London model [Eq. (6)]. Reproduced from Ref. [6], Copyright © 2009 American Physical Society.

With the increasing field, the VL Bragg peaks move out in reciprocal space and their intensities decrease, and as a consequence fewer peaks are visible. What ultimately limits how many peaks can be imaged is the vanishing intensity and imperfect background subtraction as seen for the (32)-reflection. To obtain the VL reflectivity the integrated intensity must be determined, most often by fitting a suitable function (in this case a Voigt) to each rocking curve and normalizing the area to the incident beam intensity. The difference in the Lorentz factor (angle between the scattering vector and the rotation axis) for the two reflections gives rise to a difference in the width of the two rocking curves, as they are cutting through the Ewald sphere at different incident angles. In the following the integrated intensity for all reflections has been corrected for this effect. The reflectivity is proportional to the square modulus of the VL form factor $F(q_{hk})$, which is the Fourier transform at wave vector q_{hk} of the two-dimensional magnetic flux modulation of the VL. The reflectivity and the form factor for a given reflection is related by

$$R_{hk} = \frac{2\pi\gamma^2\lambda_n^2 t}{16\phi_0^2 q_{hk}} |F(q_{hk})|^2 \tag{5}$$

where $\gamma = 1.91$ is the magnetic moment of the neutron in nuclear magnetons, t is the sample thickness, and q_{hk} is the magnitude of the scattering vector [52]. For a well-ordered VL, the magnitude of $F(q_{hk})$ is related to λ and ξ, and by a careful measurement in absolute units it is possible to obtain estimates of the characteristic length scales in the superconductor under investigation.

Since the vortex spacing depends on the magnetic field it is possible to determine the VL form factor continuously over wide range of scattering vectors. Figure 8(b) shows the field dependence of $F(q_{10})$, obtained from the integrated rocking curves and utilizing Eq. (5), compared to theoretical models for the field distribution in the mixed state. By far the simplest model is based on the London model, extended by a Gaussian cut-off to take into account the finite extent of the vortex cores [53, 54]:

$$F(q) = \frac{B}{1+(\lambda q)^2}\, \mathrm{e}^{-c(\xi q)^2} \tag{6}$$

Here the constant c is typically taken to be between 1/4 and 2 [53]. Since $(\lambda q)^2 \gg 1$ for all relevant fields the prefactor in Eq. (6) reduces to $\phi_0/(2\pi\lambda)^2$. As shown by the solid line in Fig. 8(b), the measured form factor is well fitted by this model which corresponds to a simple exponential decrease with increasing field ($q_{10}^2 \propto B$). Using $c = 1/2$ the exponential fit to the form factor yields $\lambda = 90.7$ nm and $\xi = 8.22$ nm. A more rigorous model for the form factor field dependence was obtained by Clem by including an effective core radius and solving the Ginzburg–Landau (GL) model [55]. This was later extended by Hao and Clem to include the suppression of the bulk order parameter due to vortex overlap [56, 57]. Fits to both of these models are also shown in Fig. 8(b). While GL theory is, strictly speaking, only valid close to the superconducting transition, these and other models have been shown to provide a reasonable approximation to more detailed numerical GL calculations valid away from T_c [53, 58, 59]. Ironically, the form factor is best described by the London model ($\chi^2 = 0.14$) compared to either the more sophisticated Clem ($\chi^2 = 0.62$)

or Hao ($\chi^2 = 1.20$) models. This emphasizes the point that any analysis of bulk measurements based on a particular theoretical model for the VL must be done with the utmost care. Finally, it is clear that measurements of $F(q_{10})$ alone provide limited insights into the VL field distribution.

4.1 Real space VL field reconstruction for $LuNi_2B_2C$

By extending measurements of the VL form factor beyond the first order Bragg reflection, it is possible to perform a more complete, model-independent analysis. Figure 8(c) summarizes the $LuNi_2B_2C$ VL form factors for all measured reflections and fields. In both the London and Clem models the only field dependence of $|F(q_{hk})|/H$ comes through the magnitude of the scattering vector, q_{hk}, and therefore the form factors would be expected to collapse onto a single curve. This is not the case for the data in Fig. 8(c), where the form factors instead follow different exponential field dependences as seen most clearly for the (10)- and (11)-reflections. Likewise, the data do not agree with the Hao model, which predicts that for a given q the form factor should increase with the decreasing field (larger indices h and k) and converge towards the value given by the Clem model as observed in niobium [56, 57]. Rather, we observe that while $|F(q_{11})|/H$ does indeed lie above $|F(q_{10})|/H$, other higher order form factors fall in between these two limiting curves. This is not surprising when one keeps in mind that $LuNi_2B_2C$, as well as the other members of the rare earth nickelborocarbide superconductors, posseses a significant in-plane anisotropy [60–70]. While it would be straightforward to incorporate an in-plane penetration depth anisotropy into the models discussed above, a model independent analysis of the data is desirable.

With the VL form factor being the Fourier transform of the magnetic field modulation, the real space field distribution can be obtained from the measured form factors by

$$B(\boldsymbol{r}) = \sum_{hk} F(\boldsymbol{q}_{hk})\, \mathrm{e}^{\mathrm{i}\boldsymbol{q}_{hk}\cdot\boldsymbol{r}} \tag{7}$$

In the case of the VL the so-called phase problem, arising from the fact that only the magnitude $|F(q_{hk})|$ is measured, is greatly simplified. As the magnetic field variation around any vortex exhibits inversion symmetry ($B(-\boldsymbol{r}) = B(\boldsymbol{r})$), the form factor must be real and the phase problem thus reduces to a sign problem. Within the London model the signs on all form factors are expected to be the same, which will be chosen as positive and correspond to having the vortex at the center of the unit cell. A more thorough justification of this choice is given in Ref. [6]. Note that $F(q_{00})$ is simply the applied magnetic field $\mu_0 H$. Figure 9(a) shows the field reconstruction obtained using Eq. (7) and the measured VL form factors for $LuNi_2B_2C$ at 0.5 T.

A measure of the in-plane anisotropy can be obtained by calculating the current flow around the vortices given by $\mu_0 \boldsymbol{J} = \nabla \times \boldsymbol{B}$. Figure 9(b) shows $|\boldsymbol{J}(\boldsymbol{r})|$ along the VL nearest neighbor direction as well as the unit cell diagonal. Using an operational definition of the coherence length (ξ_J) as the distance from the vortex center to the maximum current [11, 71], it is clear that this differs for the two directions shown. The inset to Fig. 9(b) shows ξ_J in the basal (screening current) plane. It is striking that the minimum ξ_J is observed along the nodal $\langle 100\rangle$-directions, where one would naively expect the weakest pairing and hence the largest ξ_J. It is also interesting to compare the field reconstruction and current profiles in Fig. 9 to the numerical work of Machida and Ichioka *et al.*, who have performed calculations for a number of VL configurations, pairing symmetries and Fermi surface anisotropies [11, 72]. From this, one finds that the best

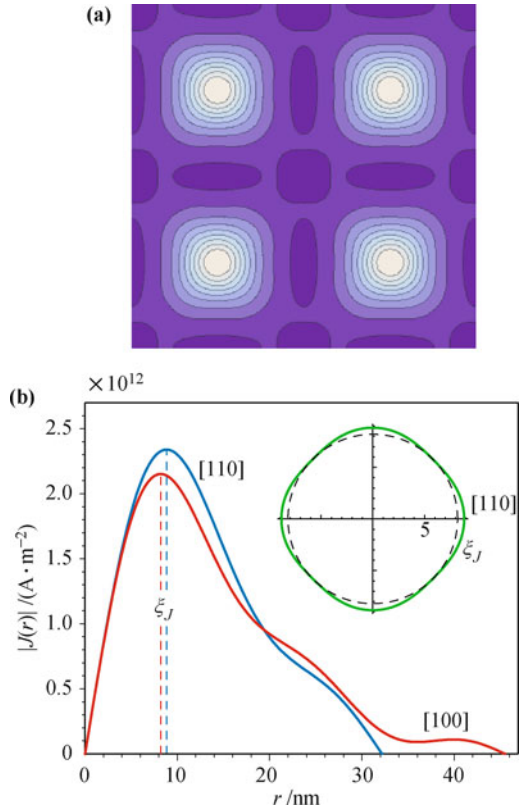

Fig. 9 Reconstruction of the real space VL field modulation in $LuNi_2B_2C$ at 0.5 T and 2 K. **(a)** Plot of the field magnitude with the lowest contour corresponding to 493 mT and an equidistant contour spacing of 5 mT. Four VL unit cells are shown, with a vortex spacing of 64.3 nm corresponding to an applied field of 0.5 T. Note that the field reconstruction images are rotated 45° with respect to the diffraction pattern in Fig. 2, so that the $\langle 110\rangle$-directions are now horizontal/vertical. **(b)** Supercurrent density as a function of distance from the vortex center, along the VL nearest neighbor vortex direction (crystalline [110] axis) and the VL diagonal (crystalline [100] axis). The inset shows the value of ξ_J (distance of maximum current) in the basal plane. To visually emphasize the four-fold anisotropy, a circle with radius $\xi_J^{[100]}$ is also shown (*dashed line*). Reproduced from Ref. [6], Copyright © 2009 American Physical Society.

agreement is achieved with an anisotropic superconducting gap (d-wave or anisotropic s-wave) combined with a Fermi surface anisotropy.

4.2 Pauli paramagnetic effects in $TmNi_2B_2C$ and $CeCoIn_5$

The exponential (or near exponential) decrease of the VL form factor with increasing field discussed above is the conventional behavior observed in the majority of superconductors. In this section, we turn to a very interesting deviation from this behavior observed in $TmNi_2B_2C$ and $CeCoIn_5$ which originates in a strong coupling between spins of the unpaired electrons in the vortex cores and the magnetism in these compounds [33, 38, 73].

The diffraction pattern in the insert to Fig. 10 shows two domains of a rhombic VL in $TmNi_2B_2C$. While the Tm moments in this material orders antiferromagnetically, the measurements described here were performed in the paramagnetic phase above $T_N = 1.5$ K. A direct measure of the magnetic induction, B, can be obtained from the VL scattering vectors. Using two scattering vectors belonging to the same domain as shown in the lower insert, the induction is given by

$$B = \frac{\phi_0}{4\pi^2}|\boldsymbol{q}_1 \times \boldsymbol{q}_2| \quad (1)$$

Figure 10 shows the measured B as a function of applied field for $TmNi_2B_2C$ with similar data for non-magnetic $LuNi_2B_2C$ included as a reference. The latter yields $\mathrm{d}B/\mathrm{d}(\mu_0 H) = 1.003 \pm 0.006$ (dashed line) as expected for a non-magnetic superconductor when $H \gg H_{c1}$. For $TmNi_2B_2C$ we find $B > \mu_0 H$ for the entire measured field range, indicating a significant paramagnetic contribution to the induction. Below ~ 0.6 T, $\mathrm{d}B/\mathrm{d}(\mu_0 H) = 1.152 \pm 0.004$ as indicated by the straight line, which is in excellent agreement with magnetization measurement when demagnetization effects is taken into account [74].

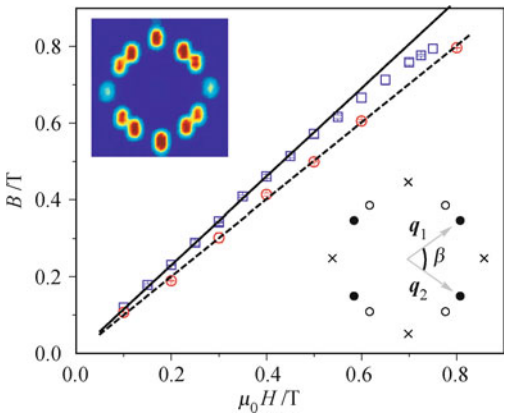

Fig. 10 Measured magnetic induction versus applied field at 1.6 K for $TmNi_2B_2C$ (*squares*) and non-magnetic $LuNi_2B_2C$ (*circles*). The top left inset shows a VL diffraction pattern obtained in $TmNi_2B_2C$ at 0.2 T and 1.6 K. The bottom right inset shows a schematic of the diffraction pattern, indicating the VL scattering vectors and opening angle. Open and closed circles represent first order VL Bragg peaks belonging to different domain orientations, while ×'es denote higher order reflections. Reproduced from Ref. [38], Copyright © 2007 American Physical Society.

We now turn to the VL form factor for $TmNi_2B_2C$ shown in Fig. 11 which is compared to the Clem model for two different choices of λ and ξ. The dotted line corresponds to a penetration depth $\lambda = 78$ nm from literature [74], and a coherence length $\xi = 21$ nm based on the measurements of the upper critical field at 1.6 K, while the dotted line is for a shorter $\lambda = 60$ nm which increases the overall magnitude of the form factor. While a good estimate of especially, the coherence length is difficult to obtain due to the suppression of H_{c2} by the paramagnetic depairing [75], it is evident that the field dependence of the calculated form factor, regardless of the choice of parameters, does not agree with the measurements. Qualitatively similar results were also obtained at temperatures further above T_N [38].

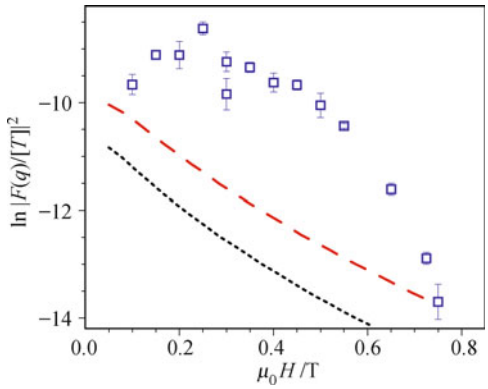

Fig. 11 Field dependendence of the measured VL form factor in $TmNi_2B_2C$ at 1.6 K. The lines show the form factor calculated using the Clem model [55] with $\xi = 21$ nm and $\lambda = 78$ nm (*dotted line*) or 60 nm (*dashed line*). Reproduced from Ref. [38], Copyright © 2007 American Physical Society.

While the clear deviation of the $TmNi_2B_2C$ VL form factor from the conventional field dependence is remarkable, an even more extreme behavior is observed in $CeCoIn_5$ [27, 33, 73]. This material exhibits clear Pauli limiting and has received considerable attention as a possible candidate to exhibit spatially inhomogenuous superconductivity known as a Fulde–Ferrell–Larkin–Ovchinnikov (FFLO) state [76, 77]. At low temperature, the transition to the normal state is first-order [78, 79], showing that the superconductivity is suppressed by the coupling of the field to the anti-parallel spins of the singlet Cooper pair (the Pauli effect) rather than the more common coupling to the orbital motion of Cooper pairs in the mixed state (orbital limiting) [80, 81]. While numerous studies report experimental signatures that are compatible with the formation of FFLO [82–87], an unambiguous microscopic observation remains elusive. Recent reports of magnetic ordering in the same low tem-

perature, high field regions of phase space where the FFLO phase is expected further complicates matters [88, 89]. However, neither of these two effects appear to couple directly to the following VL results.

In Fig. 12(a) we show the field-dependence of the $CeCoIn_5$ VL form factor for temperatures between 50 mK and 1.25 K. At all temperatures, it initially rises with increasing field before reaching a maximum, and then begins to fall again on approaching H_{c2}. At temperatures $\leqslant$ 500 mK the form factor remains finite all the way up to H_{c2} where the VL signal disappears abruptly upon entering the normal state. This is consistent with the first-order nature of the superconducting transition seen in thermodynamic measurements at low temperatures [78, 79], and predicted theoretically for strong Pauli-limiting [81]. Above 500 mK, the field-dependence begins to resemble that of $TmNi_2B_2C$, smoothly approaching zero at H_{c2} as expected for a second-order transition to the normal state. However, even at these higher temperatures, Pauli-paramagnetic effects remain important, leading to a maximum at intermediate fields. Finally we note that

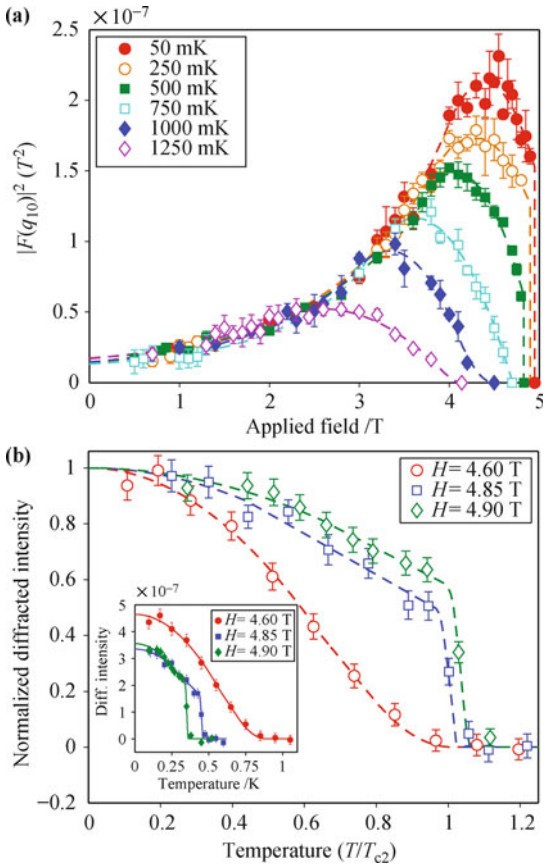

Fig. 12 VL form factor in $CeCoIn_5$. **(a)** Field-dependence of the square of the form factor for first-order Bragg reflections. The points at which the form factor goes to zero are obtained from measurements of H_{c2} [90]. **(b)** Normalized temperature-dependence of the diffracted intensity at the peak of the rocking curve for a first-order hexagonal VL Bragg spot lying along ⟨110⟩. The inset shows the same data in absolute (un-normalized) units of counts per standard monitor. Reproduced from Ref. [73], Copyright © 2010 Institute of Physics.

at low fields the form factor has a common value independent of temperature. This shows that the effects of Pauli limiting are small at low fields, and that orbital-limiting effects are fairly temperature-independent for $T \lesssim T_c/2$.

Figure 12(b) shows the detailed temperature dependence of the normalized form factor at three fields in the high field hexagonal VL phase. While the temperature scans at 4.90 and 4.85 T pass through H_{c2}, almost parallel to the upper critical field phase boundary, there is still a sharp fall in intensity when the scans cross the first-order transition to the normal state. At 4.60 T a slower and smoother variation with temperature is seen, reflecting the second-order transition at H_{c2}. One also notes that the form factor is at its maximum at the lower of the three fields which is deeper within the mixed state, as shown by the absolute data in the inset, and that it falls as either field or temperature is increased towards H_{c2}.

The unusual field dependence of the VL form factor in both $TmNi_2B_2C$ and $CeCoIn_5$ can be understood in terms of Pauli paramagnetic effects on the unpaired electrons in the vortex cores, as first proposed by Ichioka and Machida [38, 91, 92]. They used an extension of the quasi-classical Eilenberger theory [93], incorporating the Pauli paramagnetic effects by adding a Zeeman energy term μB where the parameter μ represents the relative strength of the paramagnetism. This leads to a polarization of the unpaired electron spins in the vortex cores arising from the spin-split states located there. As a result there is a spatially varying paramagnetic moment which adds to the orbital contribution to the field variation in the mixed state, giving rise to an increase in the field modulation and hence the form factor. The reason that this effect, which is not commonly observed, is so prominent in the two compounds discussed here is believed to be a strong exchange coupling of the conduction electron and the $TmNi_2B_2C$ and $CeCoIn_5$ sublattice moments. The Pauli paramagnetic effects may also provide an explanation for the re-entrant square vortex phase discussed in Section 3.1. Upon approaching H_{c2} the paramagnetic depairing causes the vortex cores to expand, indicated by the decrease in the form factor [72]. This makes the cores more isotropic, thus suppressing the anisotropy which stabilized the square VL.

Besides the polarization of the unpaired electrons in the vortex cores, the Pauli paramagnetic effects also lead to a suppression of H_{c2}, relative to the value corresponding to pure orbital limiting, which provides an independent estimate on the value of the parameter μ. In the case of $TmNi_2B_2C$ a very good agreement was found between the estimated μ and the calculated and measured form factors at three different temperatures ranging from just above T_N to $\sim 0.5T_c$ [38]. However, in the case of $CeCoIn_5$, there is only a qualitative agreement between the model calculations and the measurements. In this

material a comparison of the estimated orbital upper critical field and the measured H_{c2} yields $\mu \simeq 1.7$, similar to that of $TmNi_2B_2C$ at 1.6 K. In contrast, $\mu \simeq 2.6$ is required to obtain a reasonable agreement with the measured form factor $CeCoIn_5$ [73]. In addition, the shape of the calculated form factor, even for the larger μ, is much more symmetric than the measurements where the maximum occurs very close to H_{c2}. Recently, it was shown that accounting for antiferromagnetic fluctuation in the vortex cores yields both a skewing and an increase of the form factor which is in better agreement with our findings [94, 95]. Further improvement may result from incorporating a more three-dimensional character of the Fermi surface of $CeCoIn_5$ [96], and/or accounting for the non-Fermi liquid behavior which is most prominent near H_{c2} [82, 97].

Finally we compare the abrupt disappearance of the $CeCoIn_5$ form factor at the first order H_{c2} to the jump in the bulk magnetization. While the field modulation due to the VL contains contributions from both the orbital screening currents and the polarization of the unpaired electron spins, the latter is by far the dominant contribution close to the upper critical field [72]. Furthermore, it is a good approximation to include only the leading order Fourier component $F(q_{10})$ in the sum in Eq. (7). Assuming that the magnetization in the vortex cores is equal to $M_{\rm normal}$ just above H_{c2}, the average magnetization in the mixed state is easily found to be $\langle \mu_0 M \rangle = M_{\rm normal} - 6|F(q_{10})|$ [73], as illustrated in Fig. 13. With the measured value of the form factor of 0.4 mT just below H_{c2}, we would thus expect a jump in magnetization of $\Delta(\mu_0 M) = 2.4$ mT. This is in very good agreement with the results of bulk magnetization measurements, which give a jump at H_{c2} of 3 mT [79].

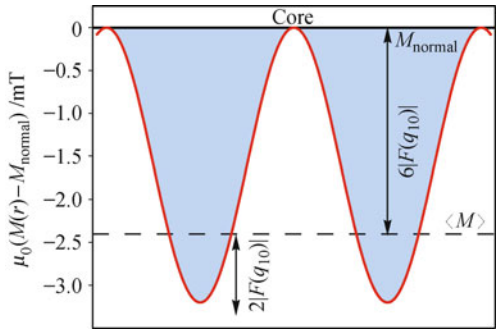

Fig. 13 Schematic of the spatial variation of the local magnetization along the nearest neighbor direction between adjacent vortex cores for an applied field just below H_{c2}. The magnetization is expected to be close to the normal state value in the cores, and decreases between the vortices where the Pauli paramagnetism is suppressed by the Cooper pairing of the supercarriers. The local magnetization varies from $+6|F(q_{10})|$ to $-2|F(q_{10})|$ relative to $\mu_0\langle M \rangle$. The shading indicates the origin of the reduced magnetization in the superconducting state. Reproduced from Ref. [73], Copyright © 2010 Institute of Physics.

5 Summary

In this mini-review we have reviewed numerous recent SANS studies of the VL in both convention and unconventional superconductors carried out by our group. The focus has been on how such measurements can provide detailed information about the nature of the superconducting state in the host material. Undoubtedly, such studies will continue to provide new and exciting results both on already known superconductors as well as those which are yet to be discovered.

Acknowledgements M. R. Eskildsen was supported by the U. S. National Science Foundation through grant DMR-0804887. Collaboration and stimulating discussions are acknowledged with: A. B. Abrahamsen, T. M. Artemova, E. D. Bauer, A. D. Bianchi, T. D. Blasius, S. L. Bud'ko, P. C. Canfield, P. Das, L. DeBeer-Schmitt, J. M. Densmore, C. D. Dewhurst, Z. Fisk, E. M. Forgan, J. L. Gavilano, S. Gerber, A. I. Goldman, M. Ichioka, R. Ikeda, N. Jenkins, M. Kenzelmann, V. G. Kogan, J. Kohlbrecher, A. Kreyssig, M. Laver, K. Machida, J. Mesot, R. Movshovich, N. Ni, T. O'Brien, C. Petrovic, R. Prozorov, K. Rovira, J. L. Sarrao, I. S. Veshchunov, L. Ya. Vinnikov, J. S. White and M. Zolliker.

References

1. A. Maisuradze, R. Khasanov, A. Shengelaya, and H. Keller, J. Phys.: Condens. Matter, 2009, 21(7): 075701
2. J. E. Sonier, W. Huang, C. V. Kaiser, C. Cochrane, V. Pacradouni, S. A. Sabok-Sayr, M. D. Lumsden, B. C. Sales, M. A. McGuire, A. S. Sefat, and D. Mandrus, Phys. Rev. Lett., 2011, 106(12): 127002
3. P. Das, J. S. White, A. T. Holmes, E. M. Forgan, A. D. Bianchi, M. Kenzelmann, M. Zolliker, S. Gerber, J. L. Gavilano, E. D. Bauer, J. L. Sarrao, C. Petrovic, and M. R. Eskildsen, to be published
4. J. S. White, V. Hinkov, R. W. Heslop, R. J. Lycett, E. M. Forgan, C. Bowell, S. Strässle, A. B. Abrahamsen, M. Laver, C. D. Dewhurst, J. Kohlbrecher, J. L. Gavilano, J. Mesot, B. Keimer, and A. Erb, Phys. Rev. Lett., 2009, 102(9): 097001
5. A. S. Cameron *et al.*, in preparation
6. J. M. Densmore, P. Das, K. Rovira, T. D. Blasius, L. DeBeer-Schmitt, N. Jenkins, D. M. Paul, C. D. Dewhurst, S. L. Bud'ko, P. C. Canfield, and M. R. Eskildsen, Phys. Rev. B, 2009, 79(17): 174522
7. A. A. Abrikosov, Sov. Phys. JETP, 1957, 5: 1174
8. W. H. Kleiner, S. H. Autler, and L. M. Roth, Phys. Rev. A, 1964, 133(5A): 1226
9. M. Franz, C. Kallin, P. I. Soininen, A. J. Berlinsky, and A. L. Fetter, Phys. Rev. B, 1996, 53(9): 5795
10. V. G. Kogan, M. Bullock, and B. Harmon, Phys. Rev. B, 1997, 55: R8693
11. M. Ichioka, A. Hasegawa, and K. Machida, Phys. Rev. B, 1999, 59(13): 8902
12. N. Nakai, P. Miranović M. Ichioka, and K. Machida, Phys. Rev. Lett., 2002, 89(23): 237004

13. K. M. Suzuki, K. Inoue, P. Miranovic, M. Ichioka, and K. Machida, J. Phys. Soc. Jpn., 2010, 79(1): 013702

14. U. Yaron, P. L. Gammel, A. P. Ramirez, D. A. Huse, D. J. Bishop, A. I. Goldman, C. Stassis, P. C. Canfield, K. Mortensen, and M. R. Eskildsen, Nature, 1996, 382(6588): 236

15. M. R. Eskildsen, P. L. Gammel, B. P. Barber, U. Yaron, A. P. Ramirez, D. A. Huse, D. J. Bishop, C. Bolle, C. M. Lieber, S. Oxx, S. Sridhar, N. H. Andersen, K. Mortensen, and P. C. Canfield, Phys. Rev. Lett., 1997, 78(10): 1968

16. Y. DeWilde, M. Iavarone, U. Welp, V. Metlushko, A. E. Koshelev, I. Aranson, G. W. Crabtree, and P. C. Canfield, Phys. Rev. Lett., 1997, 78(22): 4273

17. M. Yethiraj, D. M. Paul, C. V. Tomy, and E. M. Forgan, Phys. Rev. Lett., 1997, 78(25): 4849

18. D. M. Paul, C. V. Tomy, C. M. Aegerter, R. Cubitt, S. H. Lloyd, E. M. Forgan, S. L. Lee, and M. Yethiraj, Phys. Rev. Lett., 1998, 80(7): 1517

19. M. Yethiraj, D. M. Paul, C. V. Tomy, and J. R. Thompson, Phys. Rev. B, 1998, 58(22): 14767

20. P. L. Gammel, D. J. Bishop, M. R. Eskildsen, K. Mortensen, N. H. Andsersen, I. R. Fisher, K. O. Cheon, P. C. Canfield, and V. G. Kogan, Phys. Rev. Lett., 1999, 82(20): 4082

21. S. J. Levett, C. D. Dewhurst, and D. M. Paul, Phys. Rev. B, 2002, 66(1): 014515

22. C. D. Dewhurst, S. J. Levett, and D. M. Paul, Phys. Rev. B, 2005, 72(1): 014542

23. M. Yethiraj, D. K. Christen, D. M. Paul, P. Miranovic, and J. R. Thompson, Phys. Rev. Lett., 1999, 82(25): 5112

24. M. Yethiraj, D. K. Christen, A. A. Gapud, D. M. Paul, S. J. Crowe, C. D. Dewhurst, R. Cubitt, L. Porcar, and A. Gurevich, Phys. Rev. B, 2005, 72(6): 060504

25. R. Gilardi, J. Mesot, A. Drew, U. Divakar, S. L. Lee, E. M. Forgan, O. Zaharko, K. Conder, V. K. Aswal, C. D. Dewhurst, R. Cubitt, N. Momono, and M. Oda, Phys. Rev. Lett., 2002, 88(21): 217003

26. M. R. Eskildsen, C. D. Dewhurst, B. W. Hoogenboom, C. Petrovic, and P. C. Canfield, Phys. Rev. Lett., 2003, 90(18): 187001

27. L. DeBeer-Schmitt, C. D. Dewhurst, B. W. Hoogenboom, C. Petrovic, and M. R. Eskildsen, Phys. Rev. Lett., 2006, 97(12): 127001

28. S. P. Brown, D. Charalambous, E. C. Jones, E. M. Forgan, P. G. Kealey, A. Erb, and J. Kohlbrecher, Phys. Rev. Lett., 2004, 92(6): 067004

29. R. Gilardi, J. Mesot, S. P. Brown, E. M. Forgan, A. Drew, S. L. Lee, R. Cubitt, C. D. Dewhurst, T. Uefuji, and K. Yamada, Phys. Rev. Lett., 2004, 93(21): 217001

30. R. Cubitt, E. M. Forgan, G. Yang, S. L. Lee, D. Paul, H. A. Mook, M. Yethiraj, P. H. Kes, T. W. Li, A. A. Menovsky, Z. Tarnawski, and K. Mortensen, Nature, 1993, 365(6445): 407

31. A. Pautrat, C. Simon, C. Goupil, P. Mathieu, A. Brulet, C. D. Dewhurst, and A. I. Rykov, Phys. Rev. B, 2007, 75(22): 224512

32. Y. Li, N. Egetenmeyer, J. L. Gavilano, N. Barisic, and M. Greven, Phys. Rev. B, 2011, 83(5): 054507

33. A. D. Bianchi, M. Kenzelmann, L. DeBeer-Schmitt, J. S. White, E. M. Forgan, J. Mesot, M. Zolliker, J. Kohlbrecher, R. Movshovich, E. D. Bauer, J. L. Sarrao, Z. Fisk, C. Petrovic, and M. R. Eskildsen, Science, 2008, 319: 177

34. C. Petrovic, P. G. Pagliuso, M. F. Hundley, R. Movshovich, J. L. Sarrao, J. D. Thompson, Z. Fisk, and P. Monthoux, J. Phys.: Condens. Matter, 2001, 13(17): L337

35. K. Izawa, H. Yamaguchi, Y. Matsuda, H. Shishido, R. Settai, and Y. Onuki, Phys. Rev. Lett., 2001, 87(5): 057002

36. A. Vorontsov and I. Vekhter, Phys. Rev. Lett., 2006, 96(23): 237001

37. M. R. Eskildsen, K. Harada, P. L. Gammel, A. B. Abrahamsen, N. H. Andersen, G. Ernst, A. P. Ramirez, D. J. Bishop, K. Mortensen, D. G. Naugle, K. D. D. Rathnayaka, and P. C. Canfield, Nature, 1998, 393(6682): 242

38. L. DeBeer-Schmitt, M. R. Eskildsen, M. Ichioka, K. Machida, N. Jenkins, C. D. Dewhurst, A. B. Abrahamsen, S. L. Bud'ko, and P. C. Canfield, Phys. Rev. Lett., 2007, 99(16): 167001

39. I. Joumard, J. Marcus, T. Klein, and R. Cubitt, Phys. Rev. Lett., 1999, 82(24): 4930

40. T. Klein, I. Joumard, S. Blanchard, J. Marcus, R. Cubitt, T. Giamarchi, and P. Le Doussal, Nature, 2001, 413(6854): 404

41. M. Laver, E. M. Forgan, A. B. Abrahamsen, C. Bowell, T. Geue, and R. Cubitt, Phys. Rev. Lett., 2008, 100(10): 107001

42. P. Das, T. O'Brien, M. Laver, C. D. Dewhurst, N. Ni, S. L. Bud'ko, P. C. Canfield, and M. R. Eskildsen, Supercond. Sci. Technol., 2010, 23(5): 054007

43. M. R. Eskildsen, L. Y. Vinnikov, T. D. Blasius, I. S. Veshchunov, T. M. Artemova, J. M. Densmore, C. D. Dewhurst, N. Ni, A. Kreyssig, S. L. Bud'ko, P. C. Canfield, and A. I. Goldman, Phys. Rev. B, 2009, 79(10): 100501

44. M. R. Eskildsen, L. Y. Vinnikov, I. S. Veshchuno, T. M. Artemova, T. D. Blasius, J. M. Densmore, C. D. Dewhurst, N. Ni, A. Kreyssig, S. L. Bud'ko, P. C. Canfield, and A. I. Goldman, Physica C, 2009, 469(9–12): 529

45. D. S. Inosov, T. Shapoval, V. Neu, U. Wolff, J. S. White, S. Haindl, J. T. Park, D. L. Sun, C. T. Lin, E. M. Forgan, M. S. Viazovska, J. H. Kim, M. Laver, K. Nenkov, O. Khvostikova, S. Kuehnemann, and V. Hinkov, Phys. Rev. B, 2010, 81(1): 014513

46. Y. Yin, M. Zech, T. L. Williams, X. F. Wang, G. Wu, X. H. Chen, and J. E. Hoffman, Phys. Rev. Lett., 2009, 102(9): 097002

47. H. Kawano-Furukawa, C. J. Bowell, J. S. White, J. L. Gavilano, A. S. C. R. W. Heslop, E. M. Forgan, A. I. K. Kihou, C. H. Lee, H. Eisaki, T. Saito, H. Fukazawa, and Y. Kohori, Phys. Rev. B, 2011, 84(2): 024507

48. D. S. Inosov, J. S. White, D. V. Evtushinsky, I. V. Morozov, A. Cameron, U. Stockert, V. B. Zabolotnyy, T. K. Kim, A. A. Kordyuk, S. V. Borisenko, E. M. Forgan, R. Klingeler, J. T. Park, S. Wurmehl, A. N. Vasiliev, G. Behr, C. D.

Dewhurst, and V. Hinkov, Phys. Rev. Lett., 2010, 104(18): 187001

49. L. DeBeer-Schmitt *et al.*, in preparation
50. L. Shan, Y. L. Wang, B. Shen, B. Zeng, Y. Huang, A. Li, D. Wang, H. Yang, C. Ren, Q. H. Wang, S. H. Pan, and H. H. Wen, Nat. Phys., 2011, 7(4): 325
51. M. R. Eskildsen, E. M. Forgan, and H. Kawano-Furukawa, Rep. Prog. Phys., 2011, 74(12): 124504
52. D. K. Christen, F. Tasset, S. Spooner, and H. A. Mook, Phys. Rev. B, 1977, 15(9): 4506
53. A. Yaouanc, P. D. deReotier, and E. H. Brandt, Phys. Rev. B, 1997, 55(17): 11107
54. M. R. Eskildsen, P. L. Gammel, B. P. Barber, A. P. Ramirez, D. J. Bishop, N. H. Andersen, K. Mortensen, C. A. Bolle, C. M. Lieber, and P. C. Canfield, Phys. Rev. Lett., 1997, 79(3): 487
55. J. R. Clem, J. Low Temp. Phys., 1975, 18(5-6): 427
56. J. Clem, in: Low Temperature Physics - LT14, edited by M. Krusius and M. Vuorio, Amsterdam: North-Holland, 1975, Vol. 2: 285–288
57. Z. D. Hao, J. R. Clem, M. W. Mcelfresh, L. Civale, A. P. Malozemoff, and F. Holtzberg, Phys. Rev. B, 1991, 43(4): 2844
58. E. H. Brandt, Rep. Prog. Phys., 1995, 58(11): 1465
59. E. H. Brandt, Phys. Rev. Lett., 1997, 78(11): 2208
60. E. Boaknin, R. W. Hill, C. Proust, C. Lupien, L. Taillefer, and P. C. Canfield, Phys. Rev. Lett., 2001, 87(23): 237001
61. H. Kim, C. D. Hwang, and J. Ihm, Phys. Rev. B, 1995, 52(6): 4592
62. S. B. Dugdale, M. A. Alam, I. Wilkinson, R. J. Hughes, I. R. Fisher, P. C. Canfield, T. Jarlborg, and G. Santi, Phys. Rev. Lett., 1999, 83(23): 4824
63. P. Starowicz, C. Liu, R. Khasanov, T. Kondo, G. Samolyuk, D. Gardenghi, Y. Lee, T. Ohta, B. Harmon, P. Canfield, S. Bud'ko, E. Rotenberg, and A. Kaminski, Phys. Rev. B, 2008, 77(13): 134520
64. I. S. Yang, M. V. Klein, S. L. Cooper, P. C. Canfield, B. K. Cho, and S. I. Lee, Phys. Rev. B, 2000, 62(2): 1291
65. A. Andreone, A. Cassinese, L. Gianni, M. Iavarone, F. Palomba, and R. Vaglio, Phys. Rev. B, 2001, 64(10): 100505
66. K. Maki, P. Thalmeier, and H. Won, Phys. Rev. B, 2002, 65(14): 140502
67. K. Izawa, K. Kamata, Y. Nakajima, Y. Matsuda, T. Watanabe, M. Nohara, H. Takagi, P. Thalmeier, and K. Maki, Phys. Rev. Lett., 2002, 89(13): 137006
68. P. Martinez-Samper, H. Suderow, S. Vieira, J. Brison, N. Luchier, P. Lejay, and P. Canfield, Phys. Rev. B, 2003, 67(1): 014526
69. P. Raychaudhuri, D. Jaiswal-Nagar, G. Sheet, S. Ramakrishnan, and H. Takeya, Phys. Rev. Lett., 2004, 93(15): 156802
70. N. L. Bobrov, S. I. Beloborod'ko, L. V. Tyutrina, I. K. Yanson, D. G. Naugle, and K. D. D. Rathnayaka, Phys. Rev. B, 2005, 71(1): 014512
71. J. E. Sonier, J. Phys. Condens. Matter, 2004, 16(40): S4499
72. K. Machida and M. Ichioka, private communication
73. J. S. White, P. Das, M. R. Eskildsen, L. DeBeer-Schmitt, E. M. Forgan, A. D. Bianchi, M. Kenzelmann, M. Zolliker, S. Gerber, J. L. Gavilano, J. Mesot, R. Movshovich, E. D. Bauer, J. L. Sarrao, and C. Petrovic, New J. Phys., 2010, 12(2): 023026
74. B. K. Cho, M. Xu, P. C. Canfield, L. L. Miller, and D. C. Johnston, Phys. Rev. B, 1995, 52(5): 3676
75. J. Jensen and P. Hedegård, Phys. Rev. B, 2007, 76(9): 094504
76. P. Fulde and R. A. Ferrell, Phys. Rev., 1964, 135(3A): A550
77. A. I. Larkin and Y. N. Ovchinnikov, Sov. Phys. JETP, 1965, 20: 762
78. A. Bianchi, R. Movshovich, N. Oeschler, P. Gegenwart, F. Steglich, J. D. Thompson, P. G. Pagliuso, and J. L. Sarrao, Phys. Rev. Lett., 2002, 89(13): 137002
79. T. Tayama, A. Harita, T. Sakakibara, Y. Haga, H. Shishido, R. Settai, and Y. Onuki, Phys. Rev. B, 2002, 65(18): 180504
80. A. M. Clogston, Phys. Rev. Lett., 1962, 9(6): 266
81. K. Maki, Phys. Rev., 1966, 148(1): 362
82. A. Bianchi, R. Movshovich, I. Vekhter, P. G. Pagliuso, and J. L. Sarrao, Phys. Rev. Lett., 2003, 91(25): 257001
83. H. A. Radovan, N. A. Fortune, T. P. Murphy, S. T. Hannahs, E. C. Palm, S. W. Tozer, and D. Hall, Nature, 2003, 425(6953): 51
84. H. A. Radovan, N. A. Fortune, T. P. Murphy, S. T. Hannahs, E. C. Palm, S. W. Tozer, and D. Hall, Nature, 2004, 427(6977): 802
85. K. Kakuyanagi, M. Saitoh, K. Kumagai, S. Takashima, M. Nohara, H. Takagi, and Y. Matsuda, Phys. Rev. Lett., 2005, 94(4): 047602
86. G. Koutroulakis and M. D. S. Jr, Phys. Rev. Lett., 2010, 104(8): 087001
87. K. Kumagai, H. Shishido, T. Shibauchi, and Y. Matsuda, Phys. Rev. Lett., 2011, 106(13): 137004
88. M. Kenzelmann, T. Strässle, C. Niedermayer, M. Sigrist, B. Padmanabhan, M. Zolliker, A. D. Bianchi, R. Movshovich, E. D. Bauer, J. L. Sarrao, and J. D. Thompson, Science, 2008, 321(5896): 1652
89. E. Blackburn, P. Das, M. R. Eskildsen, E. M. Forgan, M. Laver, C. Niedermayer, C. Petrovic, and J. S. White, Phys. Rev. Lett., 2010, 105(18): 187001
90. A. Bianchi, R. Movshovich, C. Capan, P. G. Pagliuso, and J. L. Sarrao, Phys. Rev. Lett., 2003, 91(18): 187004
91. M. Ichioka and K. Machida, Phys. Rev. B, 2007, 76(6): 064502
92. V. P. Michal and V. P. Mineev, Phys. Rev. B, 2010, 82(10): 104505
93. G. Eilenberger, Z. Phys., 1968, 214(2): 195
94. R. Ikeda, Y. Hatakeyama, and K. Aoyama, Phys. Rev. B, 2010, 82(6): 060510
95. K. Aoyama and R. Ikeda, arXiv:1107.5577v1, 2011
96. R. Settai, H. Shishido, S. Ikeda, Y. Murakawa, M. Nakashima, D. Aoki, Y. Haga, H. Harima, and Y. Onuki, J. Phys. Condens. Matter, 2001, 13(27): L627
97. M. A. Tanatar, J. Paglione, C. Petrovic, and L. Taillefer, Science, 2007, 316(5829): 1320